water

MDPI

Article

Experimental Evidence of the Influence of Recurves on Wave Loads at Vertical Seawalls

Dimitris Stagonas [1,*], Rajendran Ravindar [2], Venkatachalam Sriram [2] and Stefan Schimmels [3]

[1] School of Water, Energy and Environment, Centre for Thermal Energy Systems and Materials, Cranfield University, College Rd, Wharley End, Bedford MK43 0AL, UK

[2] Department of Ocean Engineering, Indian Institute of Technology, Madras, Chennai 600036, India; itsravindar@gmail.com (R.R.); vsriram@iitm.ac.in (V.S.)

[3] Forschungszentrum Kuste (FZK), Leibniz University Hannover & Technische Universität Braunschweig, Merkurstraße 11, D-30419 Hannover, Germany; schimmels@fzk.uni-hannover.de

* Correspondence: D.Stagonas@Cranfield.ac.uk

Received: 21 December 2019; Accepted: 13 March 2020; Published: 21 March 2020

Abstract: The role of recurves on top of seawalls in reducing overtopping has been previously shown but their influence in the distribution and magnitude of wave-induced pressures and forces on the seawall remains largely unexplored. This paper deals with the effects of different recurve geometries on the loads acting on the vertical wall. Three geometries with different arc lengths, or extremity angles (α_e), were investigated in large-scale physical model tests with regular waves, resulting in a range of pulsating (non-breaking waves) to impulsive (breaking waves) conditions at the structure. As the waves hit the seawall, the up-rushing flow is deflected seawards by the recurve and eventually, re-enters the underlying water column and interacts with the next incoming wave. The re-entering water mass is, intuitively, expected to alter the incident waves but it was found that the recurve shape does not affect wave heights significantly. For purely pulsating conditions, the influence of α_e on peak pressures and forces was also negligible. In marked contrast, the mean of the maximum impulsive pressure and force peaks increased, even by a factor of more than two, with the extremity angle. While there is no clear relation between the shape of the recurve and the mean peak pressures and forces, interestingly the mean of the 10% highest forces increases gradually with α_e and this effect becomes more pronounced with increasing impact intensity.

Keywords: recurves; recurve geometry; vertical seawalls; wave loads and pressures; pulsating and impulsive conditions

1. Introduction

Wave recurves and parapets are used to reduce overtopping without considerably increasing the seawall height. The primary purpose of a recurve is to deflect the wave rushing up the wall seawards, thereby reducing overtopping. Compared with parapets, recurves form a smoother angle with the vertical wall and deflect the flow gradually. In contrast, chamfered parapets form a sharp angle with the seawall and rapidly alter the flow trajectory. Figure 1 shows the functional principle of a recurve and two examples for a sea wall equipped with a recurve and a chamfered parapet, respectively.

In Figure 2, the working principle of a recurve is further illustrated by some snapshots taken during the present experiments. It is seen how a wave is (a) approaching the sea wall and (b) hits the sea wall, producing an up-rushing water jet. The recurve (c) alters the trajectory of the up-rushing water, which is deflected seawards and (d) eventually re-enters the underlying water column and interacts with the next incoming wave (the latter interaction is not visible in Figure 2).

The positive effect of recurves and parapets in reducing overtopping has been illustrated for a range of coastal defences. [1,2] provided results showing overtopping reduction when parapets

are installed on sea-dikes. After analysing small-scale test data with recurves and parapets on a vertical seawall, [3,4] found the performance of such elements in reducing overtopping depends on the freeboard (R_c) to significant wave height (H_s) ratio. Specifically, overtopping becomes negligible for non-dimensional freeboard (R_c / H_s) values of 1.5 and higher, while for ratios less than 1.2, the positive effect of the parapet vanishes. It is also noteworthy that several seawall shapes were proposed, where the vertical wall is completely replaced by a curved wall (recurve walls) to mimic the action of recurves and reduce overtopping, e.g., [5–8].

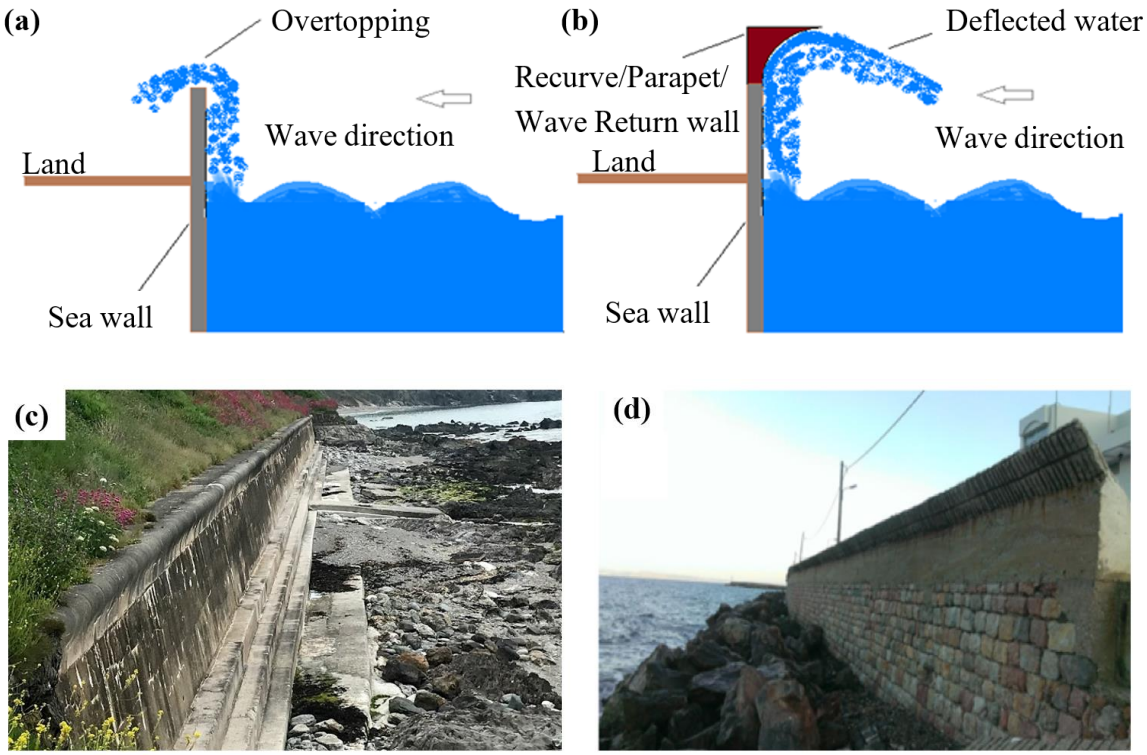

Figure 1. Schematic of the operation principle of a seawall equipped with a recurve, (**a**,**b**) and photographs of a seawall equipped with a recurve (**c**) and a chamfered parapet (**d**).

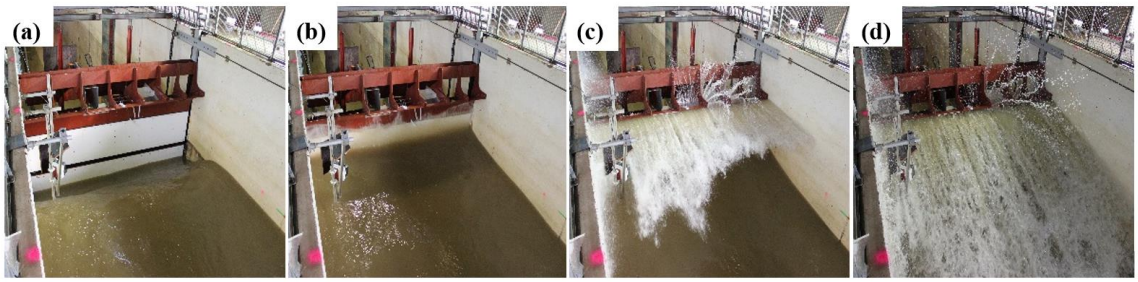

Figure 2. Sequence of snap-shots (from **a**–**d**) from the present experiments showing a wave approaching and interacting with a vertical seawall with a recurve on top.

Compared with the good understanding of the effect of recurves and parapets on the reduction of overtopping rates at vertical seawalls, much less is known about the loads on these structures, which, therefore, are often estimated by experience. Based on large-scale experiments with different recurves on a vertical seawall, [9] describe increasing wave-induced loads on the super-structure with increasing seawards protruding length, i.e., increasing extremity angle, of the recurve. Later, [10] conducted small-scale experiments for measuring the loads of non-breaking waves on recurves at the top of vertical breakwaters and also found a protruding length—wave load effect, similar to that of [9].

In this context, it is important to distinguish between pulsating loads caused by non-breaking waves where the water just goes up and down the wall and impulsive loads caused by breaking or broken waves when a more or less vertical wall of water or a mixture of air and water hits the wall, producing large pressure and force peaks and a water jet rushing vertically upwards. While the experiments of [9] covered both cases [10] were mainly focused on pulsating conditions even if [11] showed by high-fidelity numerical simulations that impulsive conditions on the recurve can be induced even by non-breaking waves.

Earlier, [3] observed that in the presence of a chamfered parapet, the wave loads acting on a model seawall increased by a factor of 1.7 and 2.0 for impulsive and pulsating conditions, respectively. These observations, however, contrasted the cases of a seawall with and without a parapet at its top, and did not consider the influence of different geometries. In addition, [3] considered the forces developed on the seawall-parapet system and not on the seawall only. At the same time, [9], [10] and [11] focused in wave pressures and loads acting on recurves with different geometries installed at the top of the same vertical wall. Therefore, and to the best of the authors' knowledge, the influence of the recurve's geometry on the pressures and loads acting on the seawall and not on the seawall-super-structure system or on the super-structure alone has seldom been considered. Given that recurves are often retrofitted on pre-existing walls, the a-priori knowledge of any influence at the loading regime on the seawall will feed into the decision-making process.

Thus, the present paper compares experimental measurements of wave loads acting on a seawall equipped with three different recurves. For the same incoming wave conditions, the shape of the recurve is altered by increasing the length of its arc, which is expressed here through the extremity angle (α_e), see Figure 3. As the extremity angle (and hence the length of the arc) increases, the protruding seaward length (B_r) of the recurve increases as well, leading to a gradual rise of the freeboard, Figure 3. Following [4], increasing the freeboard improves the overtopping performance of the recurve. In the present work, the freeboard for all three α_e considered ensures optimum overtopping performance for all recurves, thereby enabling the comparison of the wave-induced loads on the seawall without the need to consider overtopping measurements.

In the remainder, the function of the different recurves and in particular, the influence of the extremity angle to the trajectory of the seawards deflected water is described first. Then, the effect of α_e to the incoming wave conditions is considered. Finally, and still with respect to α_e, measurements of the pressure distribution and the horizontal force at the seawall are presented and discussed. At this point, it should be noted that due to the time restrictions, the case of a recurve-free vertical wall was not considered in the experiments, and this might be considered as a limitation of the present work. However, as the present study is focused on the inter-comparison of different recurve shapes and their general effect on the wave loads at a vertical wall, we believe that it is justified not to consider the pure wall case in this context.

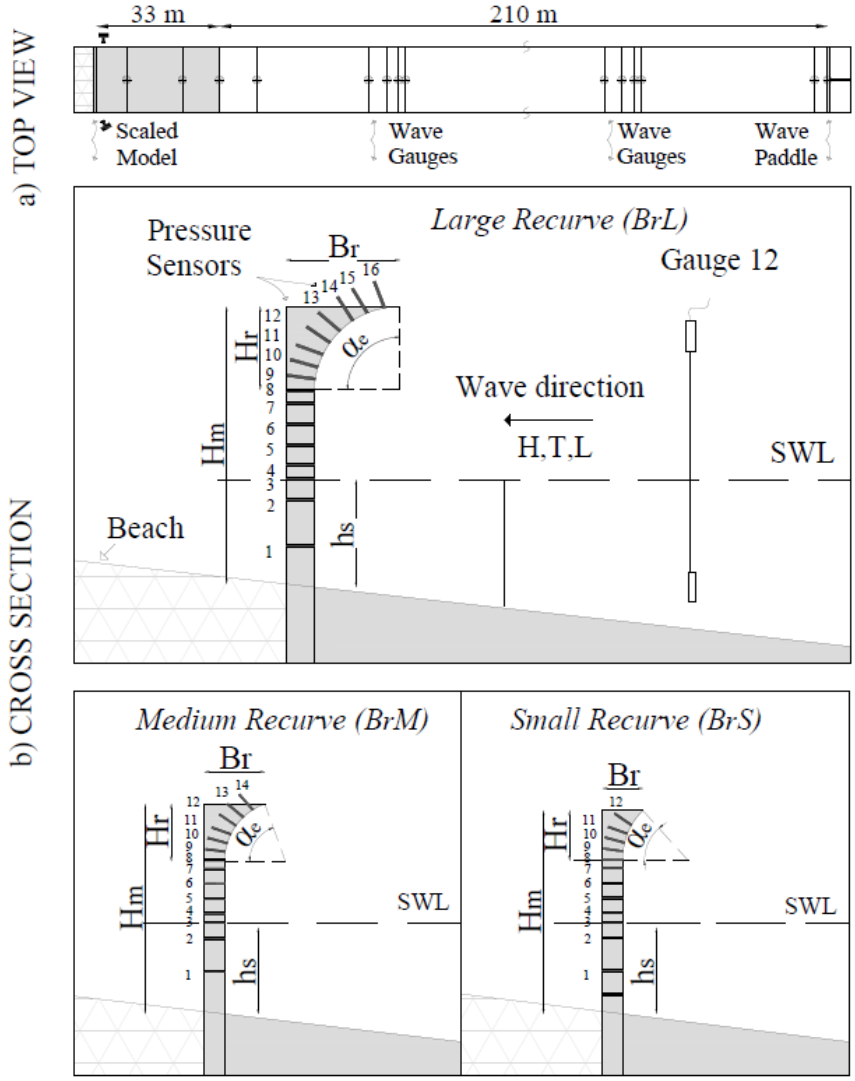

Figure 3. Experimental setup and instrumentation of the seawall and the recurves; (**a**) top view and (**b**) cross section.

2. Experimental Setup

The experiments were carried out in the Large Wave Flume (Großer Wellenkanal, GWK), Hannover, Germany. The flume is about 300 m long, 5 m wide, and 7 m deep and waves are generated by a piston-type wavemaker equipped with active wave absorption. A model seawall was installed at a distance of 243 m from the wave maker, at the end of a 33 m long 1:10 approaching slope. Twelve capacitance type, wave gauges were used to measure surface elevation in the flume, with a sampling rate of 100 Hz. Figure 3 illustrates the experimental setup.

On top of the steel-made sea wall, three different recurves with varying extremity angle (α_e), i.e., different protruding lengths B_r, were installed, giving special attention to eliminate any discontinuities at the interface between the wall and the super-structure. The three different geometries considered were as follows:

Small recurve (B_rS): $\alpha e = 48°$, $B_r = 0.20$ m, Hr = 0.45 m, Hm = 1.84 m

Medium recurve (B_rM): $\alpha e = 70°$, $B_r = 0.40$ m, Hr = 0.57 m, Hm = 1.96 m

Large recurve (B_rL): $\alpha e = 90°$, $B_r = 0.61$ m, Hr = 0.61 m, Hm = 2.00 m

Experiments were initially conducted with the small recurve B_rS, followed by tests with the medium B_rM and the large recurve B_rL. In total, 16 pressure transducers sampled at 5 kHz were used

to measure pressures on the seawall and the recurves. Seven of these transducers were located on the seawall, and 5, 7 and 9 transducers were installed in the small, medium, and large recurve, respectively.

The total horizontal force on the seawall is computed from the pressure measurements as follows:

$$F_h = \sum_j P_j \times \Delta z_j \quad (1)$$

P_j: Pressure recorded by the transducer j, with $j = 1 \ldots 7$.

Δz_j: Distance between two successive transducers on the seawall. For the lowest transducer ($j = 1$), Δz_1 is the distance between the toe of the wall and the transducer.

It is reminded that for the calculation of the horizontal force, only pressure measurements from transducers 1 to 7 were used. Therefore, F_h is the (shoreward) force acting solely on the vertical seawall and not on the whole seawall-recurve system.

Finally, two video cameras were used to record the interaction of the incoming waves with the wall and the recurves. Camera 1 was positioned inside the flume, facing the seawall at an angle, while camera 2 was placed outside and over the flume, facing its sidewall. The first camera (Camera 1) recorded videos with 300 fps and the second (Camera 2) with 30 fps.

3. Testing Conditions

Experiments were carried out at a water depth of d = 4.1 m, i.e., a water depth of h_s = 0.8 m at the toe of the wall. Six regular wave cases are considered for the present study with incident wave heights (H_i) and periods (T_i) ranging between 0.5 m < H_i < 0.8 m and 4 s < T_i < 8 s. These conditions were selected to yield non-dimensional freeboard to wave height ratios falling within the optimum overtopping performance range according to Kortenhaus et al. (2002) and resulting in both, pulsating and impulsive conditions at the vertical wall.

Table 1 summarises the wave conditions for the six cases and outlines observations made during the tests and later through the analysis of the video footage. It can be seen that the testing conditions vary from pulsating to impulsive cases, i.e., from non-breaking to plunging with small and large air pockets.

Table 1. Summary of the wave conditions. The wave height and period correspond to the target values, while the wavelength is calculated at the deep section of the flume (d = 4.1 m).

Test Case	Wave Height (m)	Wave Period (s)	Wave Length (m)	Wave Steepness	Load Condition	Observations
H07T4	0.7	4	21.02	0.033	Pulsating	Non-breaking waves running up and down the vertical wall.
H05T8	0.5	8	48.55	0.01	Pulsating	Non-breaking waves running up and down the vertical wall
H06T6	0.6	6	35.13	0.017	Pulsating (transition to impulsive)	Waves slightly breaking on the vertical wall, i.e., breaking cannot be clearly observed in the flume, but the pressure signals show an initial peak, which is higher than the following quasi-static peak. This case can be considered as transition from pulsating to impulsive conditions.
H06T8	0.6	8	48.55	0.012	Impulsive	Waves breaking on the slope, about 15 m in front of the wall. When the post-breaking wave reached the vertical wall, it overturned again and broke on the structure, forming a large air pocket between the plunging crest and the vertical wall.

Table 1. *Cont.*

Test Case	Wave Height (m)	Wave Period (s)	Wave Length (m)	Wave Steepness	Load Condition	Observations
H07T8	0.7	8	48.55	0.014	Impulsive	Waves breaking on the slope as above, but with more intense breaking of the secondary wave on the seawall.
H07T6	0.7	6	35.13	0.02	Impulsive	The wave crest overturned directly at the wall, forming a large air pocket between the wave and the structure and leading to considerable impacts with loud noise and vibrations transmitted through the structure and the flume. This case also showed the highest velocities of the up-rushing aerated water jet.

In each test, about 100 waves were generated, but for the following analysis of the surface elevation and pressure measurements, the first and last parts of the time histories were omitted, i.e., only measurements acquired after the establishment of quasi-steady conditions in the flume were considered. The minimum number of omitted waves was 15 on each side of the time history and was varied depending on the incoming wave conditions and the conditions at the wall (pulsating or impulsive).

4. Influence of the Recurve on the Incoming Wave Conditions

In all cases, pulsating and impulsive, the water mass that runs up the wall is deflected by the recurve and re-enters the underlying water surface at a certain distance in front of the wall. The angle of deflection corresponds to the angle of the recurve and during the experiments, the distance of re-entry was physically observed to vary between less than 10 m and 23 m for the cases considered here. The distance is related to the deflection angle and the speed of the up-rushing water mass at the wall, where the latter depends on the incoming wave conditions and is naturally higher for impulsive conditions than for pulsating conditions. The largest distance of about 23 m, therefore, occurred for case H07T6 and the shortest recurve B_rS, i.e., most intense breaking on the wall and an extremity/deflection angle of about 48°.

The deflected water mass surely disturbs the incoming waves, but a more detailed analysis of this interaction was beyond the scope of the present study, not at least as in most of the cases the point of re-entry was out of the field of view of the video cameras. However, in order to assess if the incoming wave conditions are differently influenced by the shape of the recurve (α_e) and by the point of re-entry relative to the phase of the incoming waves, the surface elevation records at 33 m (toe of the approaching slope) and 9 m (closest wave probe to the seawall) in front of the structure were analyzed.

In terms of the elevation record analysis, a zero down-crossing approach was used to calculate the wave period and height of each wave in every record. Then, the statistical properties of each file—e.g., the mean wave height and the standard deviation—were calculated for the part of the record corresponding to quasi-stable conditions in the flume, as explained previously. The ratio of the mean wave height nearest to the wall (H_{234}) over the mean wave height at the beginning of the slope (H_{210}) is plotted over α_e in Figure 4.

At first sight, a clear difference between the wave height ratios can be observed, which reflects the combined effects of shoaling and breaking on the slope (cases H06T8 and H07T8 only) and in particular, the re-entering water mass deflected from the structure. More importantly, the results in Figure 4 do not indicate any significant influence of α_e on the incoming wave heights, with some cases being slightly more influenced than others. However, this might also be attributed to the breaking of the approaching wave on the slope in front of the last wave probe (H_{234}), at least for H06T8 and H07T8. Overall, the height of the incoming waves does not seem to strongly depend on the shape of the recurve, i.e., the re-entry point.

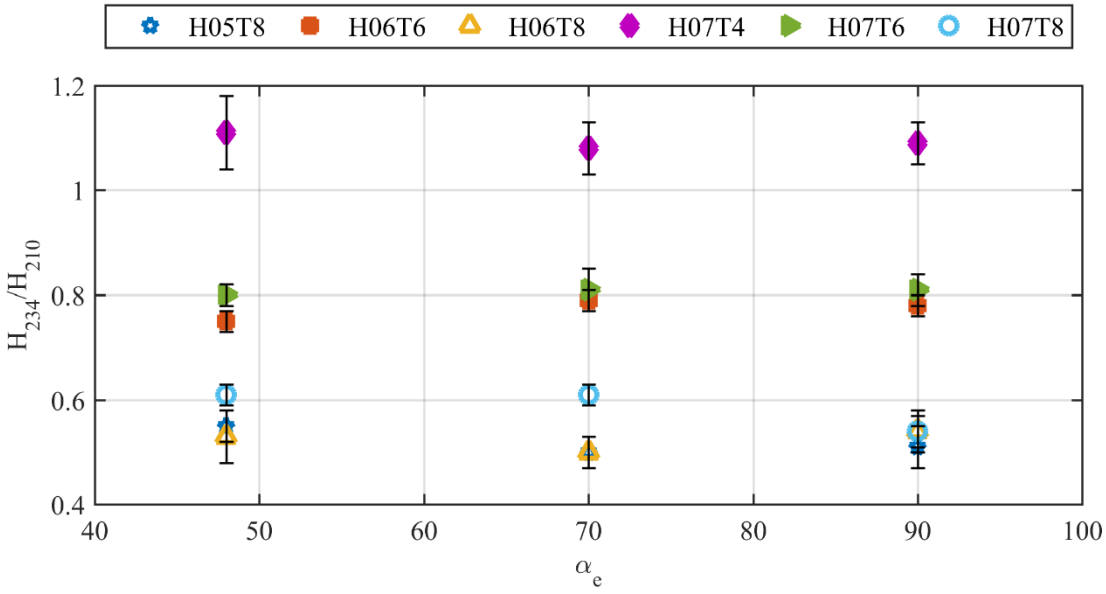

Figure 4. Ratio of mean wave heights close to the wall (H_{234}) and at the toe of the slope (H_{210}) against the extremity angle of the recurve for all test cases.

Nonetheless, the rather small differences in the incoming wave heights for the three recurve geometries do not automatically entail similar small differences for the pressures and forces on the wall. In particular, for impulsive conditions, a small change of the hydrodynamic conditions close to the wall may lead to slightly different breaking conditions, which in turn, may have a considerable impact on the wave-induced pressure and force distributions and magnitudes. This shall be further explored in the following sections considering pulsating and impulsive conditions separately.

5. Pulsating Conditions

The three test cases H07T4, H05T8 and H06T6 were considered as pulsating, while H07T4, H05T8, corresponded to waves that did not break on the seawall and H06T6 resulted in slightly breaking waves at the structure and can, therefore, be considered as transitional to impulsive conditions (cf. Table 1). According to [12], waves breaking slightly on a vertical wall induce a short first peak in the pressure time series, which is a few times larger than the following quasi-static peak. An example of such pressure records for H06T6 is shown in Figure 5.

The distribution of peak pressures along the vertical wall for all three wave conditions and all three recurves is shown in Figure 6. The colours indicate the wave conditions; green: H07T4, red: H05T8, blue H06T6, and the markers indicate the different recurve shapes; diamond: B_rS, cross: B_rM, circle: B_rL. Additionally, the pressure distribution curve proposed by [13] is also plotted (original: dashed-dotted black line; with factor 3: dashed-dotted dark grey line). While Figure 6 shows the peak pressures for each single wave, Figure 7 shows the mean values and a separate plot for each wave condition.

The highest pressure peaks occur above the still water level for all cases, which is in qualitative agreement with the observations of [14] and an indication of pulsating conditions. While the distribution of peak pressures is quite similar for all test cases, the magnitude of the pressure peaks differs considerably with the incoming wave conditions. In particular, the steeper but purely pulsating waves (H07T4) yield the smallest pressures on the wall, while less steep waves (H06T6) breaking slightly on the wall result in the highest pressure peaks, as could be expected from Figure 6. For the non-breaking wave cases (H07T4 and H05T8), some events were also significantly higher than the quasi-static pressure (Figure 6), indicating slightly breaking and deviation from purely pulsating conditions for those particular waves. However, these events occurred rather rarely for H07T4 and

slightly more often for H05T8, confirming the quite good agreement of the mean pressure peaks with the empirical pressure distribution curve proposed by [13] for H07T4 and the slightly higher values for H05T8 (Figure 7).

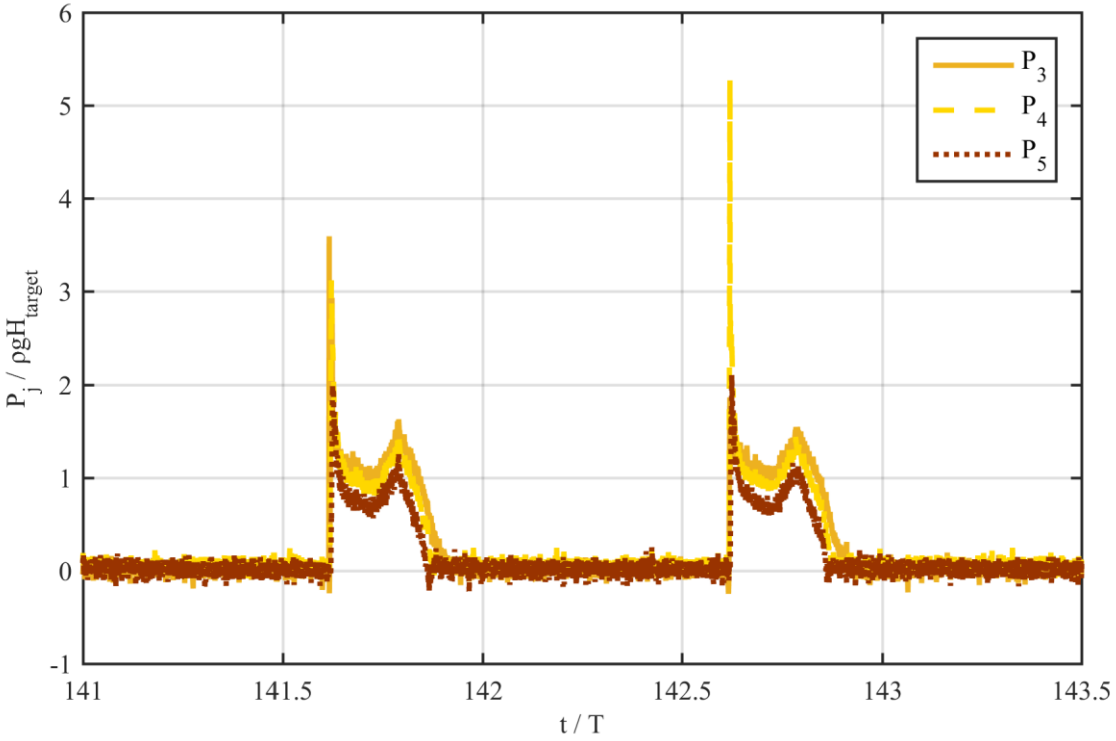

Figure 5. Example pressure time histories at three different locations on the seawall (see also Figure 3) for test case H06T6. Pressure is normalized with hydrostatic pressure of the target wave height (0.6 m), and time with wave period (6 s).

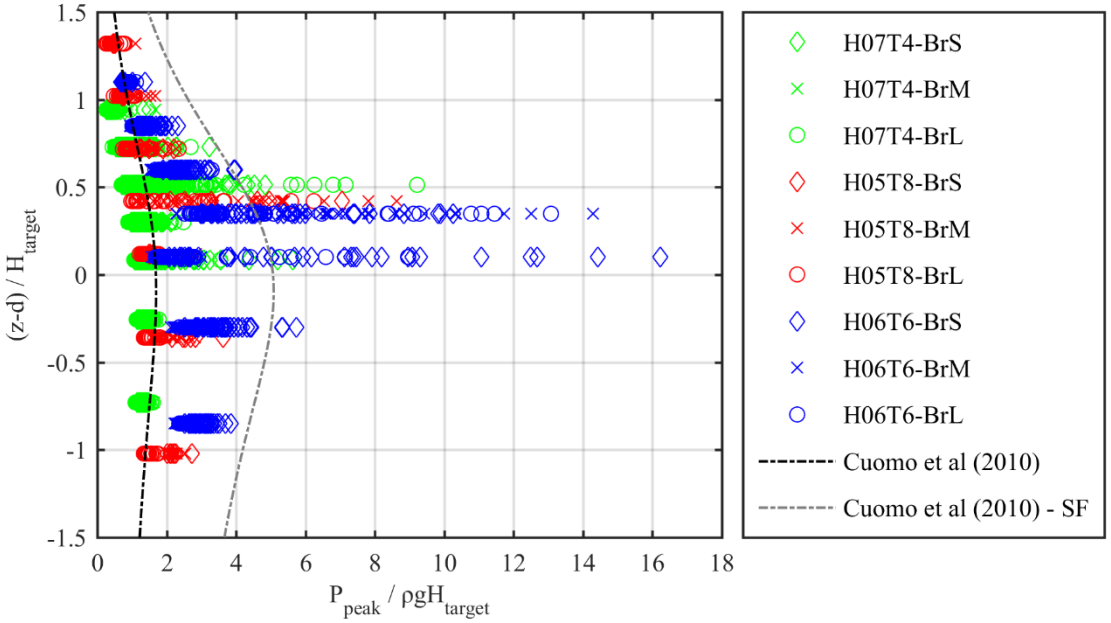

Figure 6. Distribution of pressure peaks over relative location of pressure transducers along the seawall for pulsating conditions.

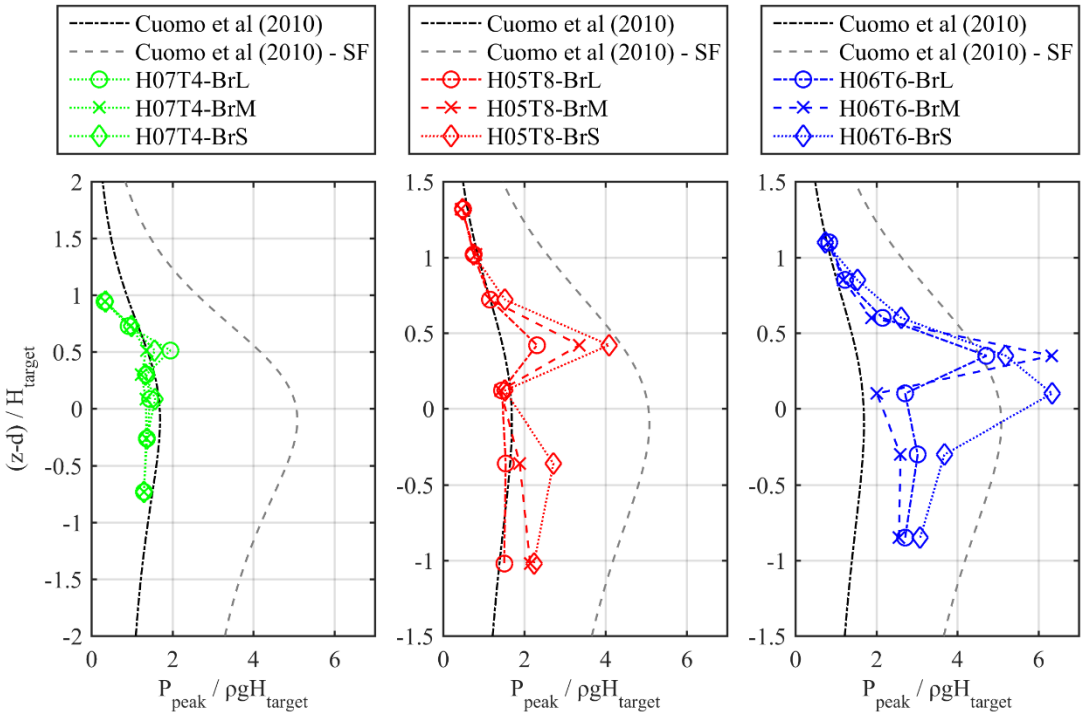

Figure 7. Mean peak pressures at each measuring location for pulsating conditions. Left: H07T4; middle: H05T8; right: H06T6.

In general, as the conditions at the wall diverge gradually from the purely pulsating regime (H07T4 → H05T8 → H06T6), the agreement with the empirical curve reduces as well. With increasing occurrence of slightly breaking waves, the highest mean peak pressures increase as expected, but also the other pressures above and below the still water level increase and the pressure distribution tends towards the empirical curve with a safety factor of 3. In particular, pressures below the still water level increase as there is also a tendency for the location of the highest peak pressures towards still water level. It should be noted here that the empirical curve of [13] was derived from experiments with irregular waves considering the mean of the highest four pressure peaks at each location and normalizing with the significant wave height H_{m0}. The safety factor of 3 was suggested as due to the random nature of irregular waves, single events were observed to be about three times larger than the values provided by the design formula. The present experiments with regular waves confirm good agreement with the design formula for purely pulsating conditions when taking the average of all pressure peaks and normalizing with the incident wave height. Furthermore, it can be noted that the re-entering of the water mass deflected by the recurve introduces a similar kind of randomness in the pressure peaks, which may exceed the mean value also by a factor of about 3.

The influence of the recurve shape can also be clearly identified in Figure 7 by the differences of the mean peak pressures, particularly at the location of the highest pressures and below. This effect increases with increasing divergence from purely pulsating conditions and can be attributed to small changes of the hydrodynamic conditions in front of the wall (cf. Section 5). Changes, which appear to depend on the location of re-entry of the deflected water mass, i.e., at which phase the incident wave is hit by the previous wave deflected from the recurve. The more severe impulsive conditions become, i.e. for more intense wave breaking, the higher and the more sensitive to local wave hydrodynamics the loads on the structure become. This is further illustrated by the mean force peaks shown in Figure 8. While basically no dependence of the forces on the extremity angle can be observed for H07T4, slight deviations can be seen for H05T8 and large differences are obvious for H06T6.

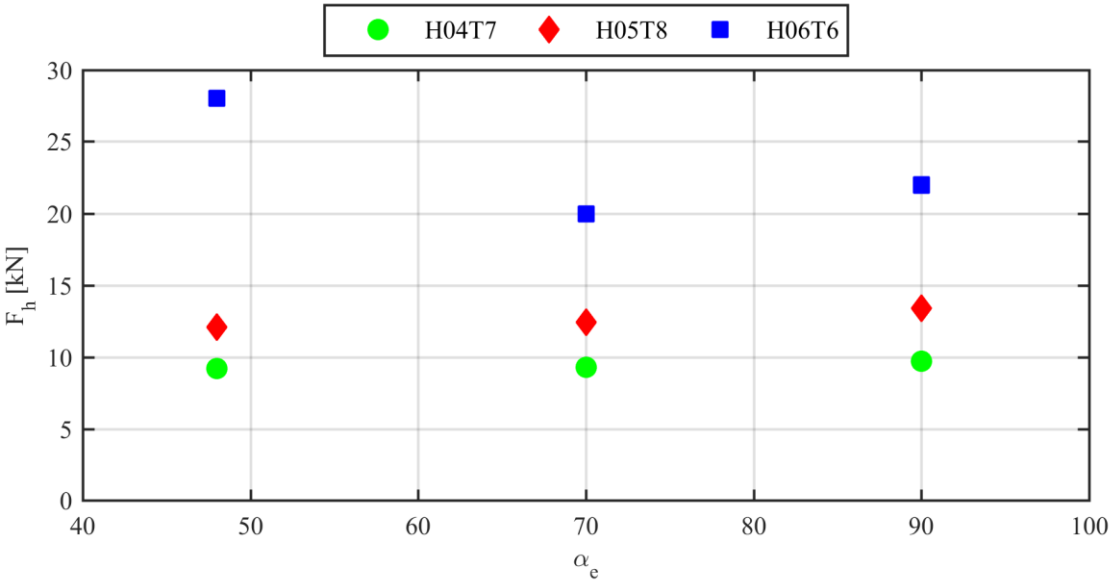

Figure 8. Mean peak force over the extremity angle of the recurve for pulsating conditions on the wall.

6. Impulsive Conditions

The location and magnitude of pressure peaks on seawalls are known to vary with the breaker type. [14], reported numerous experimental observations showing the location of maximum pressures to occur just above the still water for nearly breaking waves, at still water level for waves breaking on the seawall and forming air pockets, and below still water level when the wave crest overturns at a distance from the wall, resulting in the interaction of a plunging bore with the structure.

For the tests presented in the current work, waves for H06T8 and H07T8 plunged on the slope approximately 15 m from the seawall. The residual wave was then observed to propagate and plunge on the wall but bellow the nominal still water level line. Hence, these cases differ from the traditionally broken wave cases where an aeriated bore interacts with the wall. On the contrary, waves for H07T6 were directly breaking on the wall, forming a large air pocket between the wave and the structure (cf. Table 1).

In analogy to the discussion on pulsating conditions above, Figure 9 shows the distribution of peak pressures along the vertical wall for all three wave conditions and all three recurves, and Figure 10 shows the mean values with separate plots for each wave condition. Colours indicate the wave conditions; green: H06T8, red: H07T8, blue H07T6, and the markers indicate the different recurve shapes; diamond: B_rS, cross: B_rM, circle: B_rL.

In agreement with [13] and [14], the highest pressure peaks were recorded at and around the still water level. Even if H06T8 and H07T8 do not represent the classical broken wave cases, the highest peak pressures are found to be below still water level with H07T8 showing significantly stronger impacts than H06T8 as the residual waves were steeper and plunged with higher intensity on the structure. Waves plunging directly on the wall (H07T6) expectedly resulted in the highest pressures, with mean values up to 50 times larger than the quasi static pressures and extreme events, almost 150 times larger.

Just as for the pulsating conditions discussed above, the effect of the recurve shape on the magnitude and distribution of peak pressures along the wall can also be clearly observed for the impulsive conditions in Figure 10. It is again basically restricted to the pressures below the location of maximum impact and it is expectedly even more remarkable than for the pulsating conditions. This confirms the sensitivity of the peak pressures to only slight differences in the local (breaking) wave hydrodynamics and explains the increasing differences with increasing impact magnitude (H06TT8 → H07T8 → H07T6). Even if case H07T6 suggests that impacts also become larger with increasing

extremity angle of the recurve, this might just be a coincidence as for the other two cases this relation cannot be observed and also, the mean force peaks do not show this dependence.

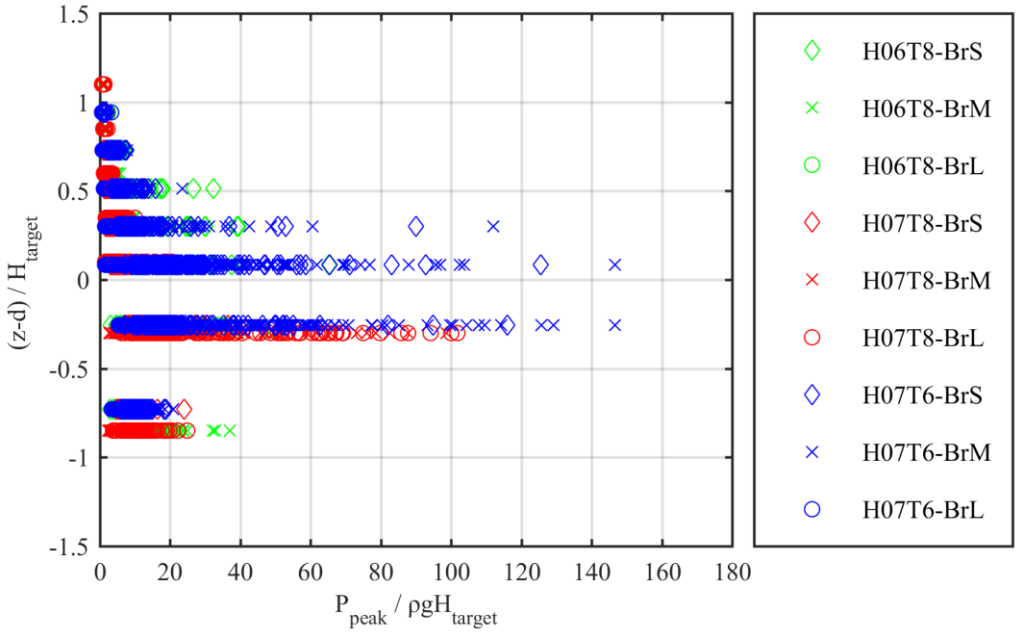

Figure 9. Distribution of pressure peaks over relative location of pressure transducers along the seawall for impulsive conditions.

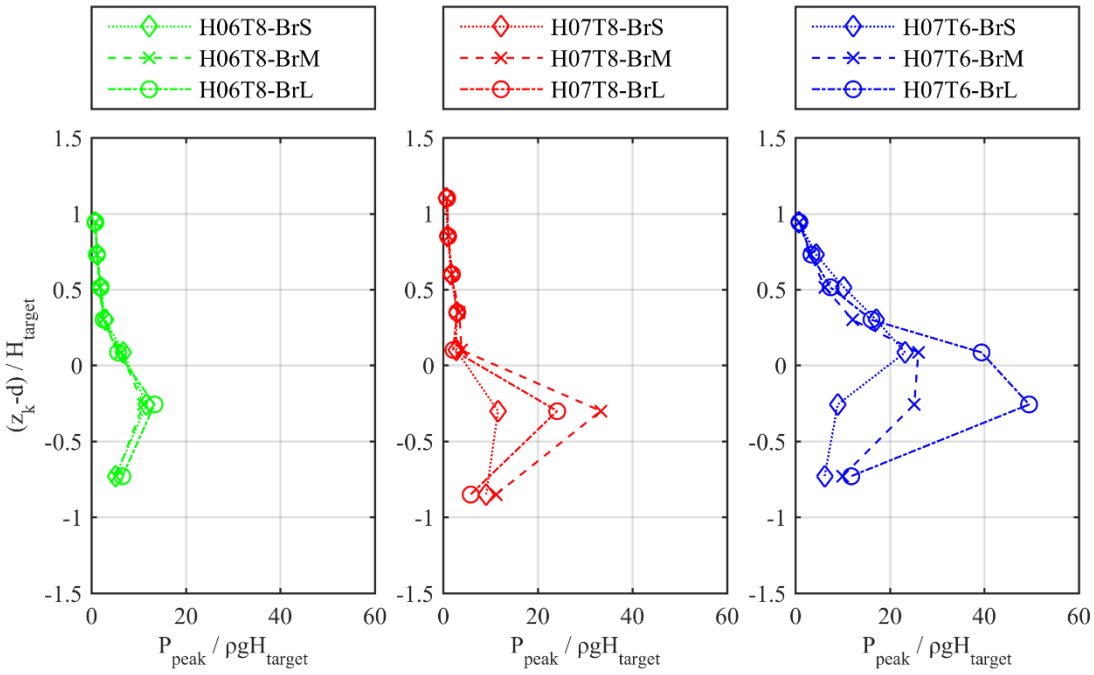

Figure 10. Mean peak pressures at each measuring location for pulsating conditions. Left: H07T4; middle: H05T8; right: H06T6.

Interestingly, this picture changes when only the largest impact events are considered. This is illustrated in Figure 11 where the mean values of the 10% highest force peaks measured on the seawall are plotted over the extremity angle (α_e). The linear trend lines have just been shown for reasons of better illustration and should in no case been interpreted as design formulas not at least as they are only valid for the particular cases considered here and they all go through the origin, implying that no

forces act on the wall without recurve ($\alpha_e = 0°$), which is surely unphysical. However, it can be clearly seen that the mean of the 10% highest force peaks increases with increasing extremity angle of the recurve for all three considered wave conditions and that this trend becomes more pronounced with increasing impact intensity. Similar results were also found when the mean of the 33% highest force peaks was considered, but it is beyond the scope of the present study to analyse this in more detail, not at least as the available data does not allow for that.

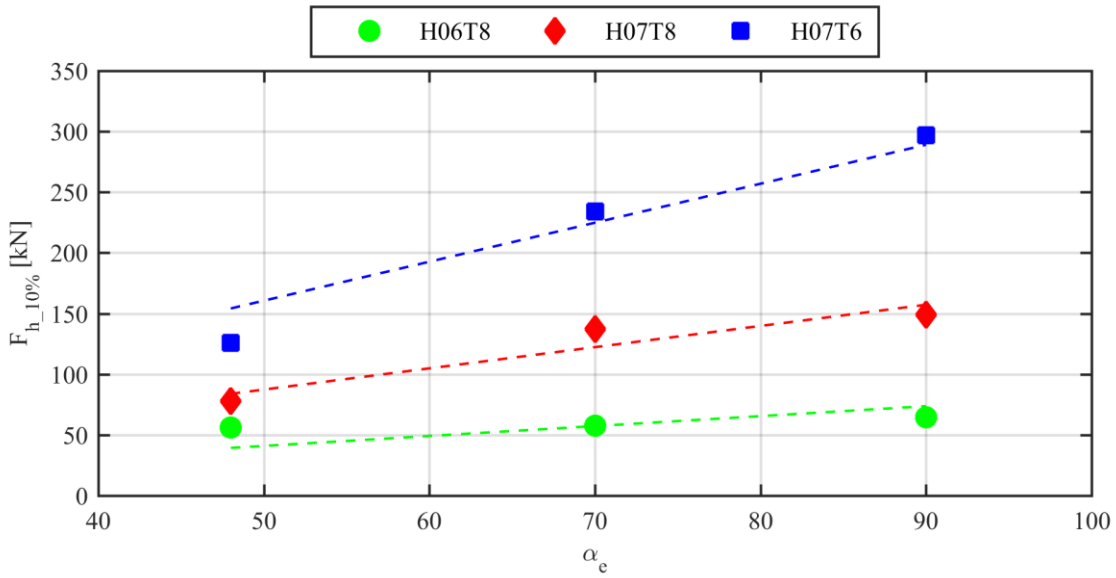

Figure 11. Mean of the 10% highest force peaks recorded for each test case over the extremity angle.

7. Conclusions

The influence of a recurve on wave-induced pressures and loads on a vertical seawall has been examined in large-scale physical model tests. Six different regular wave conditions ranging from pulsating (non-breaking) to impulsive (breaking) wave loads on the structure have been considered and three different recurves with extremity angles of 48° (B_rS), 70° (B_rM) and 90° (B_rL) were tested under the same wave conditions. The water mass running up the vertical wall is deflected by the recurve and re-enters the water in front of the structure at different distances depending on the wave conditions and the extremity angle of the recurve. Although the re-entering water mass may indeed alter the incident waves, the surface elevation measurements presented indicate that the effect of the recurve shape on the incoming wave heights is insignificant. On the other hand, pressures and forces on the vertical wall may change considerably with the recurve shape. While for purely pulsating conditions almost no influence of the recurve extremity angle can be considered, α_e becomes increasingly significant for impulsive conditions. There is no clear relation between the extremity angle of the recurve and the mean peak pressures and forces, but it was found that the mean of the largest force peaks increases with increasing α_e. Characteristically, for the same wave conditions, the mean of the 10% highest force peaks (e.g., $F_{10\%}$) may differ by a factor of more than two when impulsive conditions occur at the seawall; although not presented here, the same behaviour was also found for the mean of the 33% highest force peaks ($F_{33\%}$). Nevertheless, this effect must be further investigated and verified in future studies.

Author Contributions: D.S.: authorship; funding; design; set-up and delivery of experiments; data analysis and presentation; editing and proof read. S.S.: co-authorship, design; set-up and delivery of experiments; data analysis and presentation. R.R.: co-authorship; data analysis and presentation; editing. V.S. co-authorship; data analysis. All authors have read and agreed to the published version of the manuscript.

Funding: Funded from HYDRALAB IV transnational access scheme, contract number 261520.

Acknowledgments: This work has been carried out in the scope of project 'Large-scale measurements of wave loads and mapping of impact pressure distribution at the underside of parapets (HyIV-FZK-06)' under the funding of HYDRALAB IV, contract number 261520. The authors would like to thank the whole team at GWK for the hospitality, technical and scientific support.

Conflicts of Interest: The authors declare that to the best of their knowledge there is no conflict of interest.

References

1. Van Doorslaer, K.; De Rouck, J. Reduction on wave overtopping on a smooth dike by means of a parapet. *Coast. Eng. Proc.* **2011**, *1*, 6. [CrossRef]
2. Veale, W.; Suzuki, T.; Verwaest, T.; Trouw, K.; Mertens, T. Integrated design of coastal protection works for Wenduine, Belgium. *Coast. Eng. Proc.* **2012**, *1*, 70. [CrossRef]
3. Kortenhaus, A.; Haupt, R.; Oumeraci, H. Design aspects of vertical walls with steep foreland slopes. In *Breakwaters, Coastal Structures and Coastlines: Proceedings of the International Conference Organized by the Institution of Civil Engineers and Held in London, UK on 26–28 September 2001*; Thomas Telford: London, UK, 2001; pp. 221–232.
4. Kortenhaus, A.; Pearson, J.; Bruce, T.; Allsop, N.W.H.; van der Meer, J.W. Influence of parapets and recurves on wave overtopping and wave loading of complex vertical walls. *Coast. Struct.* **2003**, 369–381. [CrossRef]
5. Owen, M.W.; Steele, A.A.J. *Effectiveness of Recurved wave Return Walls*; HR Wallingford: Wallingford, UK, 1993.
6. Murakami, K.; Irie, I.; Kamikubo, Y. Experiments on a non-wave overtopping type of seawall. *Coast. Eng. Proc.* **1996**, *1*, 1840–1851.
7. Kamikubo, Y.; Murakami, K.; Irie, I.; Hamasaki, Y. Transportation of water spray on non-wave overtopping type seawall. In Proceedings of the Twelfth International Offshore and Polar Engineering Conference, Kitakyushu, Japan, 26–31 May 2002; Volume 3, pp. 821–826.
8. Allsop, N.W.H.; Alderson, J.S.; Chapman, A. Defending buildings and people against wave overtopping. In Proceedings of the Conference on Coastal Structures, Venice, Italy, 2–4 July 2007.
9. Stagonas, D.; Lara, J.L.; Losada, I.J.; Higuera, P.; Jaime, F.F.; Muller, G. Large scale measurements of wave loads and mapping of impact pressure distribution at the underside of wave recurves. In Proceedings of the HYDRALAB IV Joint User Meeting, Lisbon, Portugal, 2–4 July 2014.
10. Martinelli, L.; Ruol, P.; Volpato, M.; Favaretto, C.; Castellino, M.; De Girolamo, P.; Franco, L.; Romano, A.; Sammarco, P. Experimental investigation on non-breaking wave forces and overtopping at the recurved parapets of vertical breakwaters. *Coast. Eng.* **2018**, *141*, 52–67. [CrossRef]
11. Castellino, M.; Sammarco, P.; Romano, A.; Martinelli, L.; Ruol, P.; Franco, L.; De Girolamo, P. Large impulsive forces on recurved parapets under non-breaking waves. A numerical study. *Coast. Eng.* **2018**, *136*, 1–15. [CrossRef]
12. Kortenhaus, A.; Oumeraci, H. Classification of wave loading on monolithic coastal structures. *Coast. Eng. Proc.* **1998**, *1*. [CrossRef]
13. Cuomo, G.; Allsop, W.; Bruce, T.; Pearson, J. Breaking wave loads at vertical seawalls and breakwaters. *Coast. Eng.* **2010**, *57*, 424–439. [CrossRef]
14. Hull, P.; Müller, G. An investigation of breaker heights, shapes and pressures. *Ocean Eng.* **2002**, *29*, 59–79. [CrossRef]